

Fulde-Ferrel-Larkin-Ovchinnikov state in a superconducting thin film attached to a ferromagnetic cluster

Shu-Ichiro Suzuki,¹ Takumi Sato,² Alexander A. Golubov,¹ and Yasuhiro Asano²

¹*MESA+ Institute for Nanotechnology, University of Twente, 7500 AE Enschede, The Netherlands*

²*Department of Applied Physics, Hokkaido University, Sapporo 060-8628, Japan*

(Dated: May 11, 2023)

We study theoretically the Fulde-Ferrell-Larkin-Ovchinnikov (FFLO) states appearing locally in a superconducting thin film with a small circular magnetic cluster. The pair potential, the pairing correlations, the free-energy density, and the quasiparticle density of states are calculated for several cluster sizes and the exchange potentials by solving the Eilenberger equation in two dimensions. The number of nodes in the pair potential increases with increasing the exchange potential and cluster size. The local FFLO states are stabilized by the superconducting condensate away from the magnetic cluster even though the free-energy density beneath the ferromagnet exceeds locally the normal-state value. The analysis of the pairing-correlation functions shows that the spatial variation of the spin-singlet s -wave pair potential generates p -wave Cooper pairs, and that odd-frequency Cooper pairs govern the inhomogeneous subgap spectra in the local density of states. We also discuss a way of detecting the local FFLO states based on the calculated quasiparticle density of states.

I. INTRODUCTION

A spin-singlet Cooper pair in the presence of a Zeeman field has the center-of-mass momentum. As a result, the superconducting pair potential oscillates in real space. Although Fulde-Ferrel¹ (FF) and Larkin-Ovchinnikov² (LO) predicted such unusual superconducting states in 1960s, corresponding superconductors have not been found for a long time. A recent experiment has suggested a possibility of the FFLO state in FeSe³. The theoretical studies^{4,5} have indicated that the oscillation of the pair potential makes the superconducting state unstable. The oscillation of the *pairing correlations*, however, has been discussed in superconductor/ferromagnet (SF) junctions^{6–10}. Although the pair potential is absent in a ferromagnet, the pairing correlations exist due to the proximity effect. The success of these studies suggests that SF junctions can be a good system for investigating the nature of the FFLO states. An experiment¹¹, for example, realizes a superconducting state under a large exchange potential in an SF hybrid, where a circular ferromagnetic cluster is attached to a superconducting thin film. The stable FFLO state can be expected locally at the superconducting area facing to the ferromagnetic cluster.

The effects of magnetic objects embedded in a superconductor on superconducting states have been studied since the 1960s. It is well-established that magnetic impurities decrease the superconducting transition temperature T_c ¹², form an impurity band below the superconducting gap^{13–16}, and are an element for realizing the topologically nontrivial superconducting state^{17,18}. These effects depend not only on the impurity concentration and the amplitude of the magnetic moments but also on the size of a magnetic object. The suppression of the pair potentials at a point-like magnetic impurity is always small^{19,20}. However, the pair potential changes the sign at a magnetic impurity with finite size^{21–23}. In a previous

paper²⁴, we showed that odd-frequency Cooper pairs surrounding the magnetic cluster are responsible for the sign change of the pair potential.^{25,26} It is widely accepted that odd-frequency Cooper pairs exist locally in various SF hybrid structures²⁷ and play an essential role in various physical phenomena. For instance, the Josephson current through a half-metallic ferromagnet^{28–34} is attributed to odd-frequency pairs staying in the ferromagnet. At present, however, the effects of odd-frequency Cooper pairs on the FFLO state have never been well understood. We address this issue in the present paper.

We study the characteristic features of the local FFLO states in a superconducting thin film with a magnetic cluster attached to it by solving Eilenberger equation in two-dimension. We numerically calculate the pair potential, the pairing correlation functions, the free-energy density, and the quasiparticle density of states for several choices of cluster size and exchange potential. The results indicate that the superconducting condensate away from the magnetic segment stabilizes the local FFLO states. We also conclude that odd-frequency Cooper pairs support the sign change of the pair potential in real space and govern the inhomogeneous subgap spectra of the local density of states (LDOS).

This paper is organized as follows. In Sec. II, we ex-

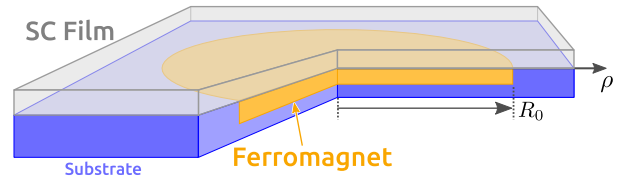


FIG. 1. Schematic picture of the system. A thin film of an s -wave superconductor is deposited on a circular-shaped magnetic cluster. The radius of the magnetic cluster R_0 is of the order of the coherence length ξ_0 .

plain a superconductor/ferromagnet structure considered in this paper and theoretical tools to analyze the superconducting states. We display the numerical results in two-dimension in Sec. III. We also discuss numerical results in one dimension in Sec. IV. The conclusion is given in Sec. V.

II. MODEL AND FORMULATION

We consider the hybrid structure shown in Fig. 1. A circular magnetic cluster is attached to an infinitely large superconducting thin film in the x - y plane. The effects of the magnetic cluster are considered through the exchange potential proximities into the superconducting film,

$$\mathbf{V}(\mathbf{r}) = V_0 \Theta(\rho - R_0) \mathbf{e}_z, \quad (1)$$

where $\rho = \sqrt{x^2 + y^2}$ and R_0 is the radius of the magnetic cluster and $\Theta(\rho)$ is the Heaviside step function. Therefore, $\rho = R_0$ indicates the boundary between the magnetic segment and the nonmagnetic segment on the superconducting thin film.

We examine the properties of the superconducting states utilizing the quasiclassical Eilenberger theory³⁵. The Green's functions obey the Eilenberger equation:

$$i\mathbf{v}_F \cdot \nabla \tilde{g} + [\tilde{g}, \tilde{H}]_- = 0, \quad (2)$$

$$\tilde{g} = \begin{pmatrix} \hat{g} & \hat{f} \\ -\hat{f} & -\hat{g} \end{pmatrix}, \quad \tilde{H} = \begin{pmatrix} \mathbf{V} \cdot \hat{\boldsymbol{\sigma}} & \hat{\Delta} \\ \hat{\Delta} & \mathbf{V} \cdot \hat{\boldsymbol{\sigma}}^* \end{pmatrix}, \quad (3)$$

where $\tilde{g} = \tilde{g}(\mathbf{r}, \mathbf{k}, i\omega_n)$ is the quasiclassical Green's function in the Matsubara representation, $\hat{\Delta}(\mathbf{r})$ is the pair potential, $\mathbf{v}_F = v_F \mathbf{k}$ is the Fermi velocity, and we assume the junction is in equilibrium. The *undertilde* function

$$\hat{\tilde{K}}(\mathbf{r}, \mathbf{k}, i\omega_n) \equiv \hat{K}^*(\mathbf{r}, -\mathbf{k}, i\omega_n), \quad (4)$$

represents particle-hole conjugation of $\hat{K}(\mathbf{r}, \mathbf{k}, i\omega_n)$, where the unit vector \mathbf{k} points the direction of the Fermi momentum. In this paper, the accents $\cdot \sim$ and $\cdot \hat{\cdot}$ means matrices in particle-hole and those in spin space, respectively. The Pauli matrices in these spaces are denoted by $\tilde{\tau}_j$ and $\hat{\sigma}_j$ with $j \in \{1, 2, 3\}$. The identity matrices are represented by $\tilde{\tau}_0$ and $\hat{\sigma}_0$. Throughout this paper, we use the system of units $\hbar = k_B = c = 1$, where k_B is the Boltzmann constant and c is the speed of light.

The Eilenberger equation (2) can be simplified by the Riccati parameterization³⁶⁻³⁹. The Green's function can be expressed in terms of the coherence function $\hat{\gamma} = \hat{\gamma}(\mathbf{r}, \mathbf{k}, i\omega_n)$:

$$\tilde{g} = 2 \begin{pmatrix} \hat{\mathcal{G}} & \hat{\mathcal{F}} \\ -\hat{\mathcal{F}} & -\hat{\mathcal{G}} \end{pmatrix} - \tilde{\tau}_3, \quad (5)$$

$$\hat{\mathcal{G}} = (1 - \hat{\gamma} \hat{\gamma})^{-1}, \quad \hat{\mathcal{F}} = (1 - \hat{\gamma} \hat{\gamma})^{-1} \hat{\gamma}. \quad (6)$$

The equation for $\hat{\gamma}$ is reduced into the Riccati-type differential equation:

$$(i\mathbf{v}_F \cdot \nabla + 2i\omega_n) \hat{\gamma} + (\mathbf{V} \cdot \hat{\boldsymbol{\sigma}}) \hat{\gamma} - \hat{\gamma} (\mathbf{V} \cdot \hat{\boldsymbol{\sigma}}^*) - \hat{\Delta} + \hat{\gamma} \hat{\Delta} \hat{\gamma} = 0. \quad (7)$$

For a spin-singlet s -wave superconductor ($\hat{\Delta} = \Delta i \hat{\sigma}_2$) under the exchange potential in Eq. (1), the anomalous Green's function and the coherence function are represented by

$$\hat{f} = i(f_0 + f_3 \hat{\sigma}_3) \hat{\sigma}_2, \quad \hat{\underline{f}} = -i \hat{\sigma}_2 (\underline{f}_0 + \underline{f}_3 \hat{\sigma}_3), \quad (8)$$

$$\hat{\gamma} = i(\gamma_0 + \gamma_3 \hat{\sigma}_3) \hat{\sigma}_2, \quad \hat{\underline{\gamma}} = -i \hat{\sigma}_2 (\underline{\gamma}_0 + \underline{\gamma}_3 \hat{\sigma}_3), \quad (9)$$

where $\underline{f}_0(\mathbf{k}) = -f_0^*(-\mathbf{k})$ and $\underline{f}_3(\mathbf{k}) = f_3^*(-\mathbf{k})$. Equation (7) can be reduced to

$$\mathbf{v}_F \cdot \nabla \gamma_0 + 2(\omega_n \gamma_0 - iV \gamma_3) - \Delta + \Delta^* [\gamma_0^2 + \gamma_3^2] = 0, \quad (10)$$

$$\mathbf{v}_F \cdot \nabla \gamma_3 + 2(\omega_n \gamma_3 - i\gamma_0 V) + \Delta^* [2\gamma_0 \gamma_3] = 0, \quad (11)$$

The coherence functions far from the magnetic cluster (i.e., $\rho \gg R_0$), $\bar{\gamma}(\mathbf{k}, i\omega_n)$ is calculated as

$$\bar{\gamma}_0 = \frac{s_\omega \Delta}{|\omega_n| + \sqrt{\omega_n^2 + |\Delta|^2}}, \quad \bar{\gamma}_3 = 0, \quad (12)$$

where $s_\omega = \text{sgn}[\omega_n]$ and $\bar{\cdot}$ means the value in the homogeneous region.

The spatial profile of the pair potential is determined by the solving the gap equation self-consistently

$$\Delta(\mathbf{r}) = 2\lambda N_0 \frac{\pi}{i\beta} \sum_{\omega_n} \langle f_0(\mathbf{r}, \mathbf{k}', i\omega_n) \rangle, \quad (13)$$

$$\lambda = \frac{1}{2N_0} \left[\ln \frac{T}{T_c} + \sum_{n=0}^{n_c} \frac{1}{n + 1/2} \right]^{-1}, \quad (14)$$

where $\beta = 1/T$, T_c is the critical temperature, N_0 is the density of the states (DOS) in the normal state at the Fermi energy, ω_c is the high-energy cut-off, and $n_c = [\omega_c/2\pi T_c]$. The angle average on the Fermi surface is denoted by $\langle \cdots \rangle = \int_{-\pi}^{\pi} \cdots d\varphi_k / 2\pi$, where $k_x = \sin \varphi_k$ and $k_y = \cos \varphi_k$ with φ_k being the azimuthal angle in the momentum space. The coordinate in real space is parameterized as $\mathbf{r} = (\rho \cos \phi_r, \rho \sin \phi_r)$. The LDOS can be calculated from the diagonal parts of the Green's function,

$$N(\mathbf{r}, \varepsilon) = N_0 \langle \text{Tr} [\hat{g}(\mathbf{r}, \mathbf{k}', i\omega_n)] \rangle|_{i\omega_n \rightarrow \varepsilon + i\delta}, \quad (15)$$

where δ is the smearing factor.

The pairing correlation function is decomposed into four dominant components. The spin-singlet s -wave com-

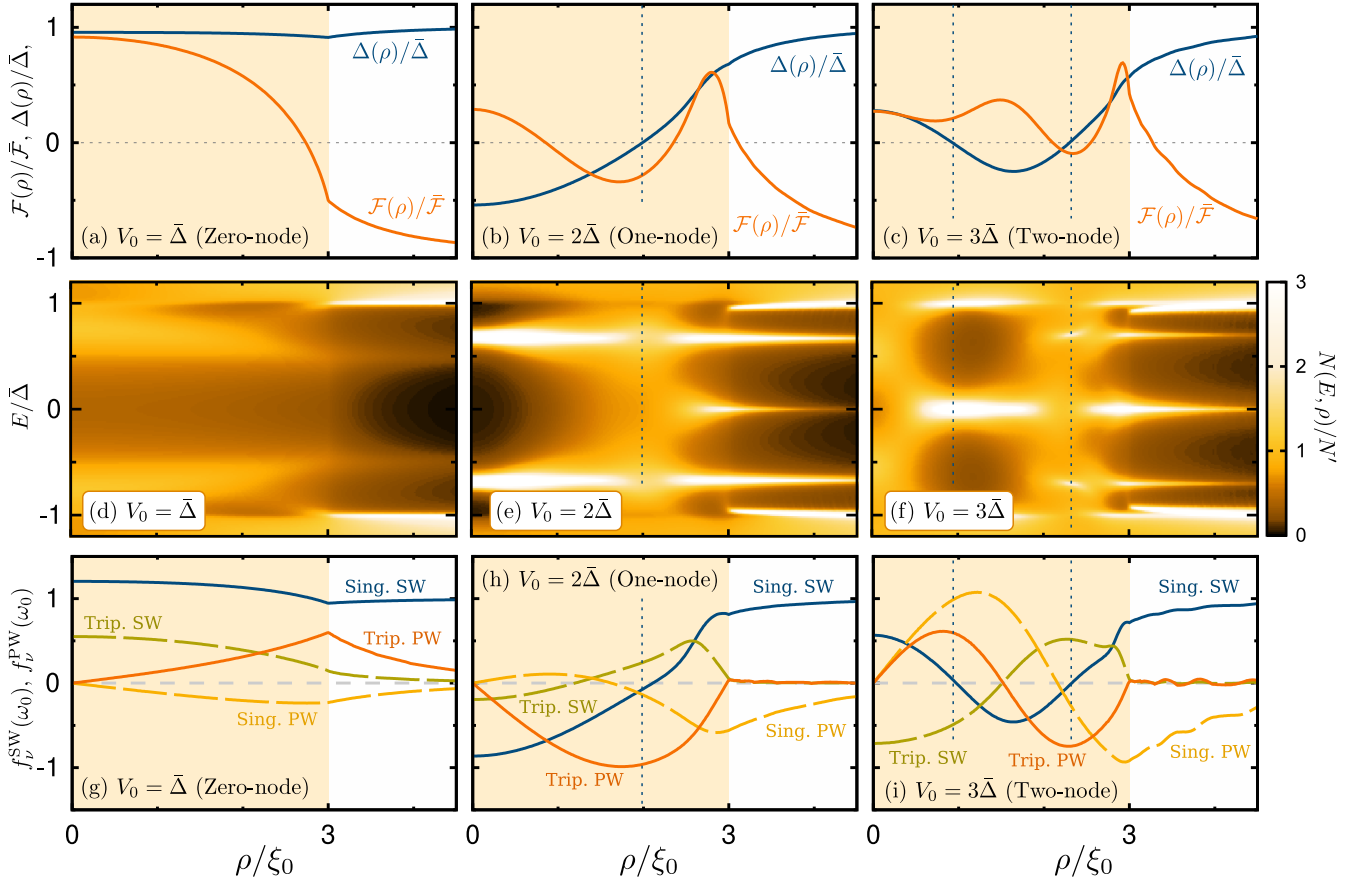


FIG. 2. Spatial profiles of the pair potential $\Delta(\rho)$ and free-energy density $\mathcal{F}(\rho)$ for (a) $V_0 = \bar{\Delta}$, (b) $2\bar{\Delta}$, and (c) $3\bar{\Delta}$. The results are normalized to their bulk values: $\bar{\Delta}$ and $\bar{\mathcal{F}}$. The positive free-energy density means that the normal state is stabler than a superconducting state locally. The vertical dotted lines indicate the places of nodes in the pair potential. The shaded areas indicate the area beneath the magnetic cluster with $R_0 = 3\xi_0$. Local densities of states (LDOS) for (d) $V_0 = \bar{\Delta}$, (e) $2\bar{\Delta}$, and (f) $3\bar{\Delta}$. The LDOS are normalised to $N' = 2N_0$. Pairing correlation functions for (g) $V_0 = \bar{\Delta}$, (h) $2\bar{\Delta}$, and (i) $3\bar{\Delta}$. The solid (broken) lines indicate the results of even-frequency (odd-frequency) pairing correlations. The temperature and the cutoff energy are set to $T = 0.2T_c$ and $\omega_c = 6\pi T_c$.

ponent

$$f_0^{\text{SW}}(\rho, i\omega) = \frac{1}{2} \langle \text{Tr}[\hat{f}(\rho, \mathbf{k}, i\omega_n)] \rangle, \quad (16)$$

is the most dominant far from the magnetic cluster and is linked to the pair potential as shown in Eq. (13). The spin-triplet s -wave component

$$f_3^{\text{SW}}(\rho, i\omega) = \frac{1}{2} \langle \text{Tr}[\hat{\sigma}_3 \hat{f}(\rho, \mathbf{k}, i\omega_n)] \rangle, \quad (17)$$

is generated by the exchange potential and belongs to odd-frequency symmetry class. In what follows, we display the calculated results at $\phi_r = 0$ because these components are isotropic in real space and independent of ϕ_r . In addition to s -wave components, odd-parity p -wave components also appear in the FFLO state since the spatial variation of the pair potential breaks inversion symmetry locally. Along the x direction $\mathbf{r} = (\rho, 0)$, two p_x -wave components are generated as a result of break-

ing inversion symmetry in the x direction: spin-singlet p_x -wave component f_0^{PW} and spin-triplet p_x -wave component f_3^{PW} defined by

$$f_\nu^{\text{PW}}(\rho, i\omega) = \frac{1}{2} \langle 2k_x \text{Tr}[\hat{\sigma}_\nu \hat{f}(\rho, \mathbf{k}, i\omega_n)] \rangle. \quad (18)$$

The free-energy density $\mathcal{F}(\mathbf{r})$ can be calculated from the Green's function as^{24,40,41},

$$\mathcal{F} = \mathcal{F}_f + \mathcal{F}_g, \quad (19)$$

$$\mathcal{F}_f = \pi N_0 T \sum_{\omega_n} \langle \Delta^*(\mathbf{r}) f(\mathbf{r}, \mathbf{k}, i\omega_n) \rangle, \quad (20)$$

$$\mathcal{F}_g = 4\pi N_0 T \sum_{\omega_n > 0} \int_{\omega_n}^{\omega'_c} \langle \text{Re}[g(\mathbf{r}, \mathbf{k}, i\omega_n) - 1] \rangle, \quad (21)$$

where the free-energy density is measured from its normal value; $\mathcal{F} = \mathcal{F}_S - \mathcal{F}_N$. In a homogeneous SC, the free-energy density approaches to $\mathcal{F}(\rho) \rightarrow -\bar{\mathcal{F}}$ at low

temperature with $\bar{\mathcal{F}} = N_0\bar{\Delta}^2/2$ being the condensation energy in the bulk.

In the numerical simulations, we fix the parameters: $\omega_c = 6\pi T_c$, $T = 0.2T_c$, $\delta = 0.01\bar{\Delta}$, and $\omega'_c = 100\bar{\Delta}$ with $\xi_0 = \hbar v_F/2\pi T_c$ being the coherence length.

III. NUMERICAL RESULTS

A. Pair potential and free-energy density

We first discuss the influences of the exchange potential on the pair potential as shown in Fig. 2(a)-(c), where the spatial variations of the pair potential are plotted for $V_0/\bar{\Delta} = 1$ in (a), 2 in (b), and 3 in (c). The size of the magnetic cluster is $R_0 = 3\xi_0$. The pair potential is almost homogeneous when the magnetization is comparable to (or smaller than) the superconducting gap (i.e., $V_0 < \bar{\Delta}$) as shown in (a). We refer to that state as the zero-node state. For $V_0 = 2\bar{\Delta}$ in (b), the pair potential is suppressed and changes its sign once around $\rho = 2\xi_0$ (one-node state). For $V_0 = 3\bar{\Delta}$ in (c), the pair potential changes the sign twice (two-node state): negative approximately at $1 < \rho/\xi_0 < 2.1$ and positive at $\rho/\xi_0 < 1$. Namely, the FFLO-like superconducting states are realized locally (i.e., only beneath the magnetic cluster).

It has been known that the uniform superconducting state under the exchange potential is possible only for $V_0 < \bar{\Delta}/\sqrt{2}$ ^{42,43}. The superconducting state for $V_0 = \bar{\Delta}$ in Fig. 2(a), however, goes over this limit. The pair potentials in Fig. 2(a)-(c) are obtained as stable self-consistent solutions of the Eilenberger equation. Such local FFLO states can be supported by the wide superconducting region outside the cluster. To confirm the validity of this argument, we calculate the free-energy density $\mathcal{F}(\rho)$ in Fig. 2(a)-(c). The vertical axis is normalized to the condensation energy in an uniform superconductor $\bar{\mathcal{F}} = \bar{\Delta}^2 N_0/2$ at zero temperature. The free-energy density outside the magnetic segment is negative (smaller than the free-energy density in the normal state) and approaches to $-\bar{\mathcal{F}}$ for $\rho \gg R_0$. Inside the magnetic segment, on the other hand, the free-energy density becomes positive locally. In particular, the free-energy density at $V_0 = \bar{\Delta}$ in Fig. 2(a) is always positive at $\rho < R_0$. However, the total free-energy $\mathcal{F}_{\text{Tot}} = \int \mathcal{F} d\mathbf{r}$ can be always negative because of the massive superconducting region outside the cluster. Figure 2(b) and (c) show that introducing the nodes into the pair potential reduces the free-energy density at $\rho < R_0$ drastically. Even so, the free energy at the magnetic segment $\mathcal{F}_{in} = \int_{r < R_0} d\mathbf{r} \mathcal{F}$ remains positive in the local FFLO states. At $V_0 = 2\bar{\Delta}$ in Fig. 2(b), \mathcal{F} has a dip at $\rho \sim 1.9\xi_0$ that corresponds to the place of the node in the pair potential. A similar behavior can be seen also in the results for $V_0 = 3\bar{\Delta}$ given in Fig. 2(c). The places of nodes in the pair potential and that of dips in the free-energy density seem to be correlated weakly to each other. This node-dip correlation, however, seems to contradict intuition. The

free-energy density would be a peak (local maximum) around a node because the quasiparticle excitations below $\bar{\Delta}$ are allowed. The results in Figure 2(b) and (c), however, show the opposite tendency. As we will discuss in Sec. III C, *p*-wave Cooper pairs stay at the nodes of the *s*-wave pair potential in real space, which affects the free-energy density.

B. Local density of states

The signs of the local FFLO state are accessible through the LDOS of a quasiparticle which can be measured by the scanning tunnel spectroscopy (STS) technique. The numerical results of the LDOS are shown in Fig. 2(d)-(f), where the exchange potentials are $V_0/\bar{\Delta} = 1$ in (d), 2 in (e), and 3 in (f). The contour plots are shown as a function of the energy of a quasiparticle E and the place ρ . At $V_0 = \bar{\Delta}$, the pair potential is almost homogeneous as shown in Fig. 2(a). The LDOS in the ferromagnetic segment indicates the appearance of quasiparticle states below the gap. The exchange potential pushes the coherence peak down to the subgap region ($|E| < \bar{\Delta}$) and broadens it in energy. As a result, the LDOS is slightly enhanced around $E = 0.7\bar{\Delta}$. These states are relating to the Yu-Shiba-Rusinov state^{13–15} localized around a point-like magnetic impurity.²⁴ The coherence peak at $|E| = \bar{\Delta}$ can be found outside the magnetic segment $\rho > R_0$. When the exchange potential increases to $V_0 = 2\bar{\Delta}$ in (e), the LDOS spectra show a complicated profile due to the spatial variation of the pair potential. The sharp subgap peak around $E = 0.7\bar{\Delta}$ exist for $0 < \rho < 1.8\xi_0$ and $\rho > 2.3\xi_0$. At the node of the pair potential $\rho = 2\xi_0$, the subgap peaks around $E = 0.7\bar{\Delta}$ are drastically suppressed and the LDOS shows almost flat spectra as it does in the normal state. The same tendency can be also seen in the results for $V_0 = 3\bar{\Delta}$ in Fig. 2(f). The spectra of LDOS for $V_0 = 3\bar{\Delta}$ in (f) become more inhomogeneous and complicated than those in (d) and (e). At the outer node at $\rho = 2.2\xi_0$, the spectra are totally flat and LDOS does not have large peaks below the gap. At the inner node at $\rho = \xi_0$, however, the LDOS has a peak at zero energy. As we will discuss in Sec. IV, the LDOS spectra changes depending sensitively on V_0 , where we display the LDOS in idealistic one-dimensional SF structures that correspond to a slice at $\phi_r = 0$ in Fig. 1.

C. Pairing correlations

We display the pairing correlation functions in Figs. 2(g)-(i) for $V_0 = \bar{\Delta}$, $2\bar{\Delta}$, and $3\bar{\Delta}$, respectively. The results are calculated for the lowest frequency at $\omega_0 = \pi T$. The spin-singlet *s*-wave component for $V_0 = \bar{\Delta}$ is always larger than other components and almost flat as shown in Figs. 2(g). Only this component has a finite amplitude far from the magnetic cluster. The two

p -wave components show a broad peak at the boundary ($\rho = R_0$) as a result of breaking inversion symmetry locally. The odd-frequency triplet s -wave component has a relatively larger amplitude than the induced p -wave components around the center. It is possible to derive the Eilenberger equation for corresponding four coherence functions: γ_0^{SW} , γ_0^{PW} , γ_3^{SW} , γ_3^{PW} . The results are displayed in Appendix . The equation at the first row of Eq. (A.5),

$$v_F k_x \frac{d}{dx} \gamma_0^{\text{SW}} + 2\omega_n \gamma_0^{\text{PW}} + 2V \gamma_3^{\text{PW}} = 0, \quad (22)$$

indicates that the spatial variation of the pair potential generates the two p -wave components γ_0^{PW} and γ_3^{PW} . In addition, the equation at the second row of Eq. (A.5),

$$v_F k_x \frac{d}{dx} \gamma_0^{\text{PW}} + 2\omega_n \gamma_0^{\text{SW}} + 2V \gamma_3^{\text{SW}} = \Delta, \quad (23)$$

explains the appearance of the spin-triplet s -wave component γ_3^{SW} even in a uniform pair potential. Here we summarize our knowledge of the relation between the frequency symmetry of a Cooper pair and their influence on the free energy and on the quasiparticle LDOS.

I Usual even-frequency pairs indicate the diamagnetic response to magnetic fields and favor the spatially uniform superconducting phase at the ground state. On the other hand, odd-frequency Cooper pairs are paramagnetic.⁴⁴ Therefore, odd-frequency pairs increase the free energy of uniform ground state⁴⁵ and favor the spatial gradient of superconducting phase²⁴.

II Even-frequency pairs support the gapped energy spectra, whereas odd-frequency pairs accompany quasiparticles below the gap.^{46,47}

These properties qualitatively explain the characteristic behavior in the free-energy density and those in the LDOS. The LDOS for $V_0 = \bar{\Delta}$ in Fig. 2(d) shows the gap-like energy spectra because even-frequency component f_0^{SW} is the most dominant everywhere. When we increase the exchange potential to $V_0 = 2\bar{\Delta}$, a node appear in the pair potential. As a consequence, the spatial profile of the pairing correlations drastically changes as shown in (h). The two p -wave components have peaks inside the boundary because the pair potential as well as the exchange potential breaks inversion symmetry locally. The amplitudes of the two p -wave components are larger than those in (g). The two spin-triplet components have large amplitudes around the node of the pair potential. The sign change of the pair potential is equivalent to the local π -phase shift in the pair potential. According to property I, odd-frequency spin-triplet s -wave components f_3^{SW} appear to decrease the free-energy density at the node of the pair potential. The triplet p -wave component f_3^{PW} is the most dominant at the node $\rho = 2\xi_0$. As a consequence, LDOS at the node in (e) does not have

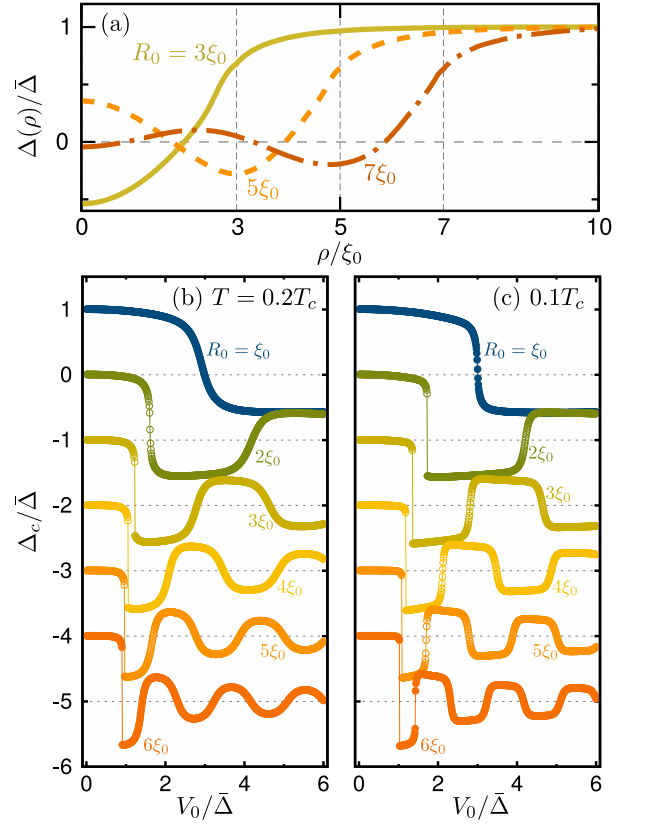


FIG. 3. (a) Cluster-size dependence of pair potentials at $V_0 = 2\bar{\Delta}$. (b,c) Pair potential at the center of the magnetic cluster ($\rho = 0$) as a function of the exchange potential V_0 . The radius of the cluster varies from $R = \xi_0$ to $6\xi_0$ by ξ_0 . The results are plotted with the offset by $(R_0/\xi_0 - 1)\bar{\Delta}$. The horizontal broken lines indicate zeros. The temperature is set to (a,b) $T = 0.2T_c$ and (c) $0.1T_c$.

large peaks below the gap. The two odd-frequency components are a source of the subgap peak at $E = 0.7\bar{\Delta}$ in (e) for $0 < \rho < 1.8\xi_0$. Outside the magnetic segment, f_0^{SW} is a source of the coherence peak at $E = \bar{\Delta}$ and f_0^{PW} assists the subgap peak at $E = 0.7\bar{\Delta}$. The two components f_0^{SW} and f_3^{PW} seem to affect the LDOS independently at $\rho > R_0$.

In a two-node state at $V_0 = 3\bar{\Delta}$, the pairing correlation functions oscillate in the ferromagnetic segment more rapidly as shown in Fig. 2(i). At the outer node $\rho = 2.2\xi_0$, the two spin-triplet components (f_3^{PW} and f_3^{SW}) fill in the blank of f_0^{SW} . The spectra of LDOS show the flat structure because the amplitude of f_3^{PW} and that of f_3^{SW} are almost the same at the outer node. Around the inner node $\rho = \xi_0$, the two odd-frequency pairing correlations dominate the two even-frequency pairing correlations. As a consequence, LDOS has a peak at zero energy for $0.7\xi_0 < \rho < 2\xi_0$. Therefore, the relative amplitudes among the four correlation functions govern the subgap spectra in the LDOS. When the odd-frequency (even-frequency) pairing correlations are dominant, the LDOS tend to have peak (gap) at $E < \bar{\Delta}$.

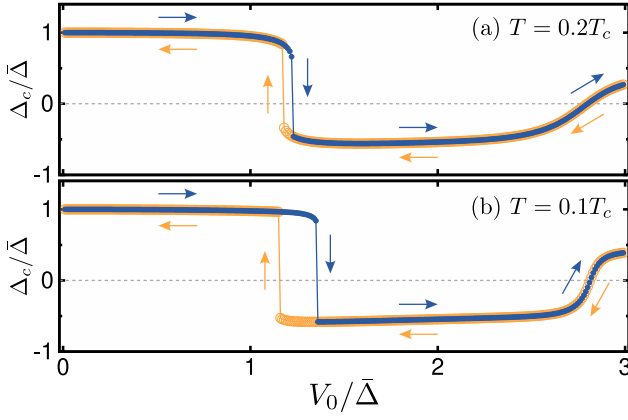


FIG. 4. Hysteresis loop of Δ_c . The degree of the hysteresis is more prominent for larger magnetic clusters and at lower temperatures. The arrows indicate how the exchange potential is changed in the numerical simulation. The radius of the island is set to $R_0 = 3\xi_0$.

At the end of this subsection, we discuss two properties of the local FFLO states. At first, the results in Figs. 2 (e) and (f), show a zero-energy state at the edge of the ferromagnetic segment $\rho = 3\xi_0 = R_0$. As we will also discussed in Fig. 6 (e) and (g) in Sec. IV, LDOS tends to have a zero-energy peak at the boundary when V_0 is close to a transition point between the n -node state and $n \pm 1$ -node state. We, however, cannot think of any reasonable explanation for why the edge states stay at zero energy. Secondly, as we already mentioned above, Eq. (22) implies that spatial variation of the singlet s -wave component (linking to the pair potential) generates two p -wave components. Simultaneously, it is possible to say that the p -wave pairing correlations drive the spatial variation in the pair potential. Therefore p -wave pairing correlations are indispensable to realizing the FFLO states. This insight suggests that the FFLO states are fragile in the presence of impurity scatterings. To our knowledge, a spin-singlet s -wave superconducting state is fragile when it contains odd-frequency pairing correlations in the clean limit^{48,49}.

D. Discontinuous transition

Figure 3(a) shows the spatial profile of the pair potential at $V_0 = 2\bar{\Delta}$, where we choose the size of the cluster as $R_0/\xi_0 = 3, 5$, and 7 . The results indicate that the multi-node states appear even with a weaker exchange potential if the radius is larger. In Figs. 3(b) and 3(c), we plot the pair potential at the center of the ferromagnetic segment $\Delta_c \equiv \Delta(\rho = 0)$, where the radius varies from $R_0 = \xi_0$ to $6\xi_0$ by ξ_0 with the corresponding offset. Changing V_0 in the horizontal axis is realized by applying an external Zeeman field in addition to the magnetic moment possessed in a ferromagnet. The pair potential keeps the homogeneous profile (i.e., $\Delta_c \approx \bar{\Delta}$ without a

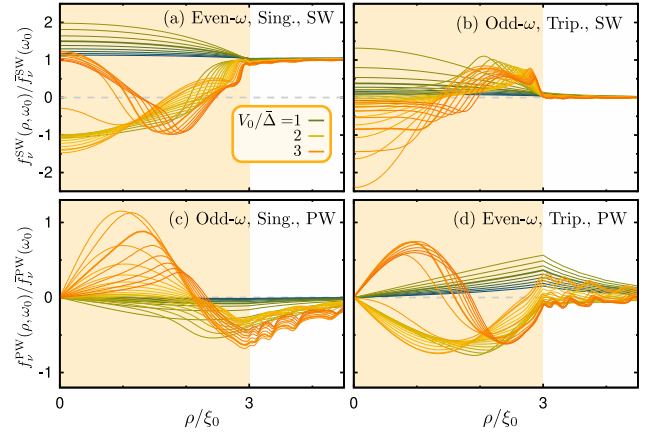


FIG. 5. Evolutions of pair amplitudes over magnetization. (a) Even-frequency spin-singlet s -wave, (b) Odd-frequency triplet s -wave, (c) Odd-frequency singlet p -wave, and (d) Even-frequency triplet p -wave are shown. The spatial profile of the pair potential is qualitatively the same as those in (a); the principal component. The magnetization varies from $V_0/\bar{\Delta} = 0.5$ to 4.0 by 0.1 . The radius of the island and the temperature are set to $R_0 = 3\xi_0$ and $T = 0.1T_c$. The even-frequency components (a,d) exhibit discrete behavior, while the odd-frequency components (b,c) vary gradually. The values of V_0 are given in the legend only for the thick lines.

node) until V_0 reaches to a critical value defined by V_1 . At $V_0 = V_1$, Δ_c changes the sign abruptly, meaning that a node appears in the pair potential. The results show a relation $V_1 \approx \bar{\Delta}$ holds $R_0 > 2\xi_0$ which limits the validity of the theoretical model for a topologically nontrivial superconducting nanowire.^{50,51} Each time Δ_c changes the sign in Fig. 3, the number of nodes in the pair potential changes by one.

We also find the jump in Δ_c at $V_0 = V_1$ shows the hysteresis between the two processes in the numerical simulation: increasing and decreasing V_0 . The results for $R_0 = 3\xi_0$ are displayed in Fig. 4, where we choose (a) $T = 0.2T_c$ and (b) $0.1T_c$. The hysteresis loop is more prominent at a lower temperature. We have confirmed that the hysteresis loop appears also between the one- and two-node states if a temperature is low enough.

By comparing Fig. 3(b) and (c), the degree of the discontinuous behavior is more remarkable at lower temperature. The first term of the Eilenberger equation in Eq. (7) is proportional to $(\partial_x + \xi_T^{-1})\hat{\gamma}$ along the x axis, where we focus on the lowest Matsubara frequency, and $\xi_T = \hbar v_F / 2\pi T$ is the thermal coherence length in the clean limit. In the equation, the influences of the spatial derivative of $\hat{\gamma}$ on the solution are more dominant for lower temperatures. In other words, the spatial variation in the coherence functions are correlated within the range of $\pi\xi_T^2$. At $T = 0.1T_c$, the thermal coherence length becomes $\xi_T = 10\xi_0$. In such a temperature, the whole area of the ferromagnetic segment is smaller than $\pi\xi_T^2$. Thus, Δ_c tends to change more abruptly at lower temperatures. Figure 3 also indicates that the disconti-

nuity between the zero-node and the one-node states is more remarkable for larger clusters. At present, however, we cannot think of reasons for this tendency.

In Fig. 5, we display the pairing correlations functions by changing the exchange potential gradually for $R_0 = 3\xi_0$. The spatial profile of spin-singlet s -wave component in the n -node state is qualitatively different from those in $n \pm 1$ -node states as shown in Fig. 5(a). Roughly speaking, the spatial profiles of f_0^{SW} is insensitive to V_0 as long as the number of nodes in the pair potential remains the same value. As a result, the calculated results for f_0^{SW} are bundled for each number of nodes. The same discontinuous tendency can be seen also in the even-frequency spin-triplet p -wave component in Fig. 5(d). Such discontinuous behavior in the pairing correlation functions is responsible for the jump of the pair potential between the n -node state and $n + 1$ -node state. The spatial profile of the two even-frequency pairing components is governed mainly by the number of nodes. The two odd-frequency components in Fig. 5(b) and (c), on the other hand, changes gradually with increasing V_0 . Consequently, odd-frequency pairs relax the effects of discontinuous change in the pair potential at the transition point. This might be a role of odd-frequency pairs in the FFLO states. The gradual change of the odd-frequency pairing correlations causes the gradual change of subgap spectra in the LDOS. We will discuss this issue in Sec. IV.

IV. ANALYSIS IN ONE-CHANNEL MODEL

The one-channel model is represented by putting $k_y = 0$ in all the equations in Sec. II and describes a one-dimensional superconducting structure including the exchange potential of $V(x) = V_0\Theta(|x| - L_0)$. Although the one-channel model is not realistic, the characteristic behaviors in the LDOS in the one-channel model are a little bit simpler than those in the two-dimension.

The pair potential at the center of the system (i.e., $\Delta_c = \Delta|_{x=0}$) is shown in Fig. 6(a) where $L_0 = 3\xi_0$ and $T = 0.2T_c$. We focus on the several characteristic exchange potentials indicated by the arrows: $V_0/\bar{\Delta} = 0.8$ (zero-node), 1.1 (just before the transition), 1.2 (just after the transition), 1.9 (one-node state), 2.9 (after the second transition), and 3.8 (two-node state). The spatial profile of the pair potentials in Fig. 6(b) is qualitatively the same as those in the 2D case [See Fig. 2(a-c)]. We have also confirmed that the transition between the one-node and two-node states becomes discontinuous at a low temperature. The LDOS calculated for these exchange potentials in Fig. 6(c-h) indicate that the quasi-particle spectra are not simply determined by the number of nodes but depend sensitively on the exchange potential. In the zero-node state in Fig. 6(c), the LDOS at the interface ($x = 3\xi_0$) has peaks around $|E| = 0.6$ and that at the center of the magnetic segment has peaks around $|E| = 0.9$. Just below the transition point to the one-

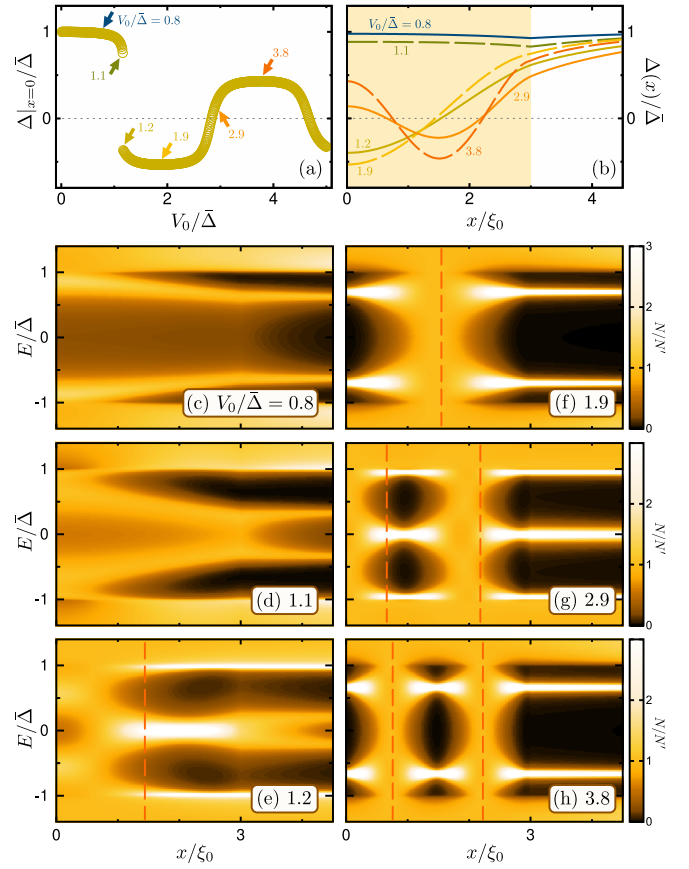


FIG. 6. Results for the one-channel model. The length of the ferromagnet and the temperature are set to $L_0 = 3\xi_0$ and $T = 0.2T_c$, respectively. (a) Pair potential at the center of the system. (b) Spatial profiles of the pair potential. (c-h) Local density of states. The magnetization is set to the characteristic values indicated by the arrows in (a): $V_0/\bar{\Delta} = 0.8$ (zero-node), 1.1 (before the transition), 1.2 (after the transition), 1.9 (one-node state), 2.9 (after the second transition), and 3.8 (two-node state). The vertical broken lines in (c-h) indicate the position of the nodes.

node state, the LDOS at the boundary ($x = 3\xi_0$) has a peak at zero energy as shown in Fig. 6(d). The zero-energy peak at the boundary can be seen also just above the transition point in Fig. 6(e) and (g). At $V_0/\bar{\Delta} = 1.9$, the one-node state is stable because the exchange potential is far from the two transition points of $V_0/\bar{\Delta} = 1.15$ and 2.85 as shown in Fig. 6(a). The corresponding LDOS in Fig. 6(f) shows that the spectra are flat $N \approx N_0$ at the node of the pair potential and gapped at the boundary. The same tendency is found also for the stable two-node states at $V_0/\bar{\Delta} = 3.8$ in Fig. 6(h). The subgap spectra in (e) and (f) are qualitatively different from each other although the pair potential in these states in Fig. 6(b) are similar to each other. As already discussed in Fig. 5, the spatial profiles of the odd-frequency components for these states deviate from each other. As a result, the subgap spectra in (e) and (f) are totally different from each other according to property II. This conclusion can

be applied also to the LDOS in the two two-node states shown in Fig. 6(g) and (h). Thus, the gradual changes of the odd-frequency pairing correlations are responsible for the gradual changes in the LDOS.

V. CONCLUSION

We have theoretically studied the property of the FFLO state which appears in a superconducting thin film attached to a circular-shaped magnetic cluster. By solving the quasiclassical Eilenberger equation, we calculate the pair potential, free-energy density, the pairing correlation functions, and the local density of states. The FFLO states are locally realized beneath the ferromagnetic cluster as a stable solution of the self-consistent gap equation. The free-energy density shows that the local FFLO states are supported by superconducting condensate surrounding the magnetic cluster. When we increase the exchange potential, the number of nodes in the pair potential increases one by one. The spatial profiles of the even-frequency pairing correlations are not sensitive to the exchange potential but is determined mainly by the number of nodes in the pair potential. On the other hand, the odd-frequency pairing correlations changes gradually with increasing the exchange potential. The local density of states is inhomogeneous in the FFLO state. In addition, its subgap spectra depend sensitively on the exchange potential because the odd-frequency pairs coexist with subgap quasiparticles.

ACKNOWLEDGMENTS

This work was supported by JSPS KAKENHI (No. JP20H01857). S.-I. S. acknowledges Overseas Research Fellowships by JSPS and the hospitality at the University of Twente. T. S. is supported in part by the establishment of university fellowships towards the creation of science technology innovation from the Ministry of Educa-

tion, Culture, Sports, Science, and Technology (MEXT) of Japan.

Appendix: Analysis in linearized Eilenberger equation

It is possible to derive the Eilenberger equation for the corresponding four coherence functions defined by

$$\gamma_0^{\text{SW}} = \frac{1}{2} \{ \gamma_0(\mathbf{k}) + \gamma_0(-\mathbf{k}) \}, \quad (\text{A.1})$$

$$\gamma_0^{\text{PW}} = \frac{1}{2} \{ \gamma_0(\mathbf{k}) - \gamma_0(-\mathbf{k}) \}, \quad (\text{A.2})$$

$$\gamma_3^{\text{SW}} = \frac{1}{2i} \{ \gamma_3(\mathbf{k}) + \gamma_3(-\mathbf{k}) \}, \quad (\text{A.3})$$

$$\gamma_3^{\text{PW}} = \frac{1}{2i} \{ \gamma_3(\mathbf{k}) - \gamma_3(-\mathbf{k}) \}. \quad (\text{A.4})$$

Here we assume that an *s*-wave (*p*-wave) component is the most dominant in an even-parity (odd-parity) coherence function. The Eilenberger equation for these components results in

$$\begin{aligned} v_F \mathbf{k} \cdot \nabla \begin{bmatrix} \gamma_0^{\text{SW}} \\ \gamma_0^{\text{PW}} \\ \gamma_3^{\text{SW}} \\ \gamma_3^{\text{PW}} \end{bmatrix} + 2 \begin{bmatrix} 0 & \omega & 0 & V \\ \omega & 0 & V & 0 \\ 0 & -V & 0 & \omega \\ -V & 0 & \omega & 0 \end{bmatrix} \begin{bmatrix} \gamma_0^{\text{SW}} \\ \gamma_0^{\text{PW}} \\ \gamma_3^{\text{SW}} \\ \gamma_3^{\text{PW}} \end{bmatrix} \\ + \begin{bmatrix} 2(\gamma_0^{\text{SW}}\gamma_0^{\text{PW}} - \gamma_3^{\text{SW}}\gamma_3^{\text{PW}}) \\ (\gamma_0^{\text{SW}})^2 + (\gamma_0^{\text{PW}})^2 - (\gamma_3^{\text{SW}})^2 - (\gamma_3^{\text{PW}})^2 \\ 2(\gamma_0^{\text{SW}}\gamma_3^{\text{PW}} + \gamma_0^{\text{PW}}\gamma_3^{\text{SW}}) \\ 2(\gamma_0^{\text{SW}}\gamma_3^{\text{SW}} - \gamma_0^{\text{PW}}\gamma_3^{\text{PW}}) \end{bmatrix} \\ = \begin{bmatrix} 0 \\ \Delta \\ 0 \\ 0 \end{bmatrix}. \end{aligned} \quad (\text{A.5})$$

The pair potential is calculated from an spin-singlet *s*-wave component γ_0^{SW} .

¹ P. Fulde and R. A. Ferrell, *Phys. Rev.* **135**, A550 (1964).

² A. I. Larkin and Y. N. Ovchinnikov, *Sov. Phys. JETP* **20**, 762 (1965).

³ S. Kasahara, Y. Sato, S. Licciardello, M. Čulo, S. Arsenijević, T. Ottenbros, T. Tominaga, J. Böker, I. Eremin, T. Shibauchi, J. Wosnitzer, N. E. Hussey, and Y. Matsuda, *Phys. Rev. Lett.* **124**, 107001 (2020).

⁴ H. Burkhardt and D. Rainer, *Annalen der Physik* **506**, 181 (1994).

⁵ S. Matsuo, S. Higashitani, Y. Nagato, and K. Nagai, *Journal of the Physical Society of Japan* **67**, 280 (1998).

⁶ L. N. Bulaevskii, V. V. Kuzii, and A. A. Sobyanin, *JETP Lett.* **25**, 291 (1977).

⁷ A. I. Buzdin, L. N. Bulaevskii, and S. V. Panyuko, *JETP Lett.* **35**, 179 (1982).

⁸ V. V. Ryazanov, V. A. Oboznov, A. Y. Rusanov, A. V. Veretennikov, A. A. Golubov, and J. Aarts, *Phys. Rev. Lett.* **86**, 2427 (2001).

⁹ T. Kontos, M. Aprili, J. Lesueur, F. Genêt, B. Stephanidis, and R. Boursier, *Phys. Rev. Lett.* **89**, 137007 (2002).

¹⁰ S. Mironov, A. Mel'nikov, and A. Buzdin, *Phys. Rev. Lett.* **109**, 237002 (2012).

¹¹ G. C. Ménard, S. Guissart, C. Brun, R. T. Leriche, M. Trif, F. Debontridder, D. Demaille, D. Roditchev, P. Simon, and T. Cren, *Nature Communications* **8**, 2040 (2017).

¹² A. A. Abrikosov and L. P. Gor'kov, *Sov. Phys. JETP* **12**, 1243 (1961).

¹³ L. Yu, *Acta. Phys. Sin* **21**, 75 (1965).

¹⁴ H. Shiba, *Progress of Theoretical Physics* **40**, 435 (1968).

¹⁵ A. I. Rusinov, *Sov. Phys. JETP Lett* **9**, 85 (1969).

- ¹⁶ A. Yazdani, B. A. Jones, C. P. Lutz, M. F. Crommie, and D. M. Eigler, *Science* **275**, 1767 (1997).
- ¹⁷ T.-P. Choy, J. M. Edge, A. R. Akhmerov, and C. W. J. Beenakker, *Phys. Rev. B* **84**, 195442 (2011).
- ¹⁸ S. Nadj-Perge, I. K. Drozdov, J. Li, H. Chen, S. Jeon, J. Seo, A. H. MacDonald, B. A. Bernevig, and A. Yazdani, *Science* **346**, 602 (2014).
- ¹⁹ A. I. Rusinov, *Sov. Phys. JETP* **29**, 1101 (1969).
- ²⁰ Y. V. Fominov and M. A. Skvortsov, *Phys. Rev. B* **93**, 144511 (2016).
- ²¹ M. I. Salkola, A. V. Balatsky, and J. R. Schrieffer, *Phys. Rev. B* **55**, 12648 (1997).
- ²² M. E. Flatté and J. M. Byers, *Phys. Rev. Lett.* **78**, 3761 (1997).
- ²³ A. V. Balatsky, I. Vekhter, and J.-X. Zhu, *Rev. Mod. Phys.* **78**, 373 (2006).
- ²⁴ S.-I. Suzuki, T. Sato, and Y. Asano, *Phys. Rev. B* **106**, 104518 (2022).
- ²⁵ D. Kuzmanovski, R. S. Souto, and A. V. Balatsky, *Phys. Rev. B* **101**, 094505 (2020).
- ²⁶ V. Perrin, F. L. N. Santos, G. C. Ménard, C. Brun, T. Cren, M. Civelli, and P. Simon, *Phys. Rev. Lett.* **125**, 117003 (2020).
- ²⁷ F. S. Bergeret, A. F. Volkov, and K. B. Efetov, *Phys. Rev. Lett.* **86**, 4096 (2001).
- ²⁸ R. S. Keizer, S. T. B. Goennenwein, T. M. Klapwijk, G. Miao, G. Xiao, and A. Gupta, *Nature* **439**, 825 (2006).
- ²⁹ Y. Asano, Y. Tanaka, and A. A. Golubov, *Phys. Rev. Lett.* **98**, 107002 (2007).
- ³⁰ Y. Asano, Y. Sawa, Y. Tanaka, and A. A. Golubov, *Phys. Rev. B* **76**, 224525 (2007).
- ³¹ V. Braude and Y. V. Nazarov, *Phys. Rev. Lett.* **98**, 077003 (2007).
- ³² J. W. A. Robinson, J. D. S. Witt, and M. G. Blamire, *Science* **329**, 59 (2010).
- ³³ T. S. Khaire, M. A. Khasawneh, W. P. Pratt, and N. O. Birge, *Phys. Rev. Lett.* **104**, 137002 (2010).
- ³⁴ M. S. Anwar, F. Czeschka, M. Hesselberth, M. Porcu, and J. Aarts, *Phys. Rev. B* **82**, 100501 (2010).
- ³⁵ G. Eilenberger, *Zeitschrift für Physik A Hadrons and nuclei* **214**, 195 (1968).
- ³⁶ N. Schopohl, arXiv:cond-mat, 9804064 (1998).
- ³⁷ N. Schopohl and K. Maki, *Phys. Rev. B* **52**, 490 (1995).
- ³⁸ M. Eschrig, *Phys. Rev. B* **61**, 9061 (2000).
- ³⁹ M. Eschrig, *Phys. Rev. B* **80**, 134511 (2009).
- ⁴⁰ G. Eilenberger, *Zeitschrift für Physik* **190**, 142 (1966).
- ⁴¹ S.-I. Suzuki and Y. Asano, *Phys. Rev. B* **91**, 214510 (2015).
- ⁴² B. S. Chandrasekhar, *Applied Physics Letters* **1**, 7 (1962), <https://doi.org/10.1063/1.1777362>.
- ⁴³ A. M. Clogston, *Phys. Rev. Lett.* **9**, 266 (1962).
- ⁴⁴ Y. Asano, A. A. Golubov, Y. V. Fominov, and Y. Tanaka, *Phys. Rev. Lett.* **107**, 087001 (2011).
- ⁴⁵ Y. Asano and A. Sasaki, *Phys. Rev. B* **92**, 224508 (2015).
- ⁴⁶ Y. Tanaka and A. A. Golubov, *Phys. Rev. Lett.* **98**, 037003 (2007).
- ⁴⁷ D. Kim, S. Kobayashi, and Y. Asano, *Journal of the Physical Society of Japan* **90**, 104708 (2021).
- ⁴⁸ Y. Asano and A. A. Golubov, *Phys. Rev. B* **97**, 214508 (2018).
- ⁴⁹ T. Sato and Y. Asano, *Phys. Rev. B* **102**, 024516 (2020).
- ⁵⁰ Y. Oreg, G. Refael, and F. von Oppen, *Phys. Rev. Lett.* **105**, 177002 (2010).
- ⁵¹ R. M. Lutchyn, J. D. Sau, and S. Das Sarma, *Phys. Rev. Lett.* **105**, 077001 (2010).